Constructing the Universe with Clusters of Galaxies, IAP 2000 meeting, Paris (France) July 2000
Florence Durret & Daniel Gerbal eds.

NONTHERMAL EMISSION FROM CLUSTERS OF GALAXIES

M. TAKIZAWA
Department of Physics, Yamagata University, Yamagata, 990-8560, Japan

We have investigated evolution of non-thermal emission from relativistic electrons accelerated at around the shock fronts during merger of clusters of galaxies. We estimate synchrotron radio emission and inverse Compton scattering of cosmic microwave background photons from extreme ultraviolet (EUV) to hard X-ray range. The hard X-ray emission is most luminous in the later stage of merger. Both hard X-ray and radio emissions are luminous only while signatures of merging events are clearly seen in thermal intracluster medium (ICM). On the other hand, EUV radiation is still luminous after the system has relaxed. Propagation of shock waves and bulk-flow motion of ICM play crucial roles to extend radio halos. In the contracting phase, radio halos are located at the hot region of ICM, or between two substructures. In the expanding phase, on the other hand, radio halos are located between two ICM hot regions and shows rather diffuse distribution.

1 Introduction

Some clusters of galaxies have diffuse non-thermal synchrotron radio halos, which extend in a $\sim$ Mpc scale (e.g., Giovannini *et al.* [4]; Röttgering *et al.* [12]; Deiss *et al.* [1]). This indicates that there exists a relativistic electron population with energy of a few GeVs (if we assume the magnetic field strength is an order of μG) in intracluster space in addition to the thermal intracluster medium (ICM). Furthermore, it is well known that such clusters of galaxies have evidences of recent major merger in X-ray observations (e.g., Markevitch, Sarazin, & Vikhlinin [7]; Watanabe *et al.* [18]). In such clusters of galaxies with radio halos, non-thermal X-ray radiation due to inverse Compton (IC) scattering of cosmic microwave background (CMB) photons by the same electron population is expected (Rephaeli [9]). Indeed, non-thermal X-ray radiation was recently detected in a few rich clusters (Fusco-Femiano *et al.* [3]) and several galaxy groups (Fukazawa [2]) although their origins are still controversial. In addition to such relatively high energy non-thermal emission, diffuse extreme ultraviolet (EUV) emission is detected from a number of clusters of galaxies (Lieu, Bonamente, & Mittaz [6]). Although their origins are also unclear, one hypothesis is that EUV emission is due to IC emission of CMB. If the hypothesis is right, this indicates existence of relativistic electrons with energy of several handled MeVs in intracluster space.

The origin of such relativistic electrons is still unclear. From N-body + hydrodynamical

simulations, it is expected that there exist shock waves and strong bulk-flow motion in ICM during merger (e.g, Schindler & Müller [14]; Ishizaka & Mineshige [5]; Takizawa [15]). This suggests that relativistic electrons are produced at around the shock fronts through 1st order Fermi acceleration and that propagation of the shock waves and bulk-flow of ICM are responsible for extension of radio halos. Obviously, the merger shock acceleration model can explicitly explain the association between merger and radio halos. However, such hydrodynamical effects on time evolution and spatial distribution of relativistic electrons during merger are not properly considered in previous studies.

In this paper, we investigate the evolution of a relativistic electron population and non-thermal emission in the framework of the merger shock acceleration model. We perform N-body + hydrodynamical simulations, explicitly considering the evolution of a relativistic electron population produced at around the shock fronts (Takizawa & Naito [16]).

2 MODELS

We consider the merger of two equal mass ($0.5 \times 10^{15} M_{\odot}$) subclusters. In order to calculate the evolution of ICM, we use the smoothed-particle hydrodynamics (SPH) method. Each subcluster is represented by 5000 N-body particles and 5000 SPH particles. The initial conditions for ICM and N-body components are the same as those of Run A in Takizawa [15]. The numerical methods and initial conditions for N-body and hydrodynamical parts are fully described in §3 of Takizawa [15]. Our code is fully 3-dimensional.

To follow the evolution of a relativistic electron population, we should solve the diffusion-loss equation for each SPH particle. Since the diffusion term is negligible, the equation is,

$$\frac{dN(E_{\rm e},t)}{dt} = \frac{\partial}{\partial E_{\rm e}}[b(E_{\rm e},t)N(E_{\rm e},t)] + Q(E_{\rm e},t), \tag{1}$$

where $N(E_{\rm e},t)dE_{\rm e}$ is the total number of relativistic electrons per a SPH particle with kinetic energies in the range $E_{\rm e}$ to $E_{\rm e}+dE_{\rm e}$ (hereafter, we denote kinetic energy of an electron to $E_{\rm e}$), $b(E_{\rm e},t)$ is the rate of energy loss for a single electron with an energy of $E_{\rm e}$, and $Q(E_{\rm e},t)dE_{\rm e}$ gives the rate of production of new relativistic electrons per a SPH particle.

According to the standard theory of 1st order Fermi acceleration, we assume that $Q(E_{\rm e},t) \propto E_{\rm e}^{-\alpha}$, where α is described as $(r+2)/(r-1)$ using the compression ratio of the shock front, r. For the shocks appeared in this simulation, the ratio is roughly $\sqrt{10}$ (Takizawa [15]), which provides $\alpha = 2.4$. The normalization of $Q(E_{\rm e},t)$ is proportional to the artificial viscous heating, which is nearly equal to the shock heating. We generate the relativistic electrons everywhere even if explicit shock structures do not appear in the simulation. We assume that sub-shock exists where a fluid element has enough viscous heating. Such sub-shocks are recognized in higher resolution simulations (e.g. Roettiger, Burns, & Stone [11]). We assume that total kinetic energy of accelerated electrons from $E_{\rm e} = 0$ to $+\infty$ is 5% of the viscous energy, which is consistent with the recent TeV gamma ray observational results for the galactic supernova remnant SN 1006 (Tanimori *et al.* [17]; Naito *et al.* [8]). Note that equation 1 for the evolution of a relativistic electron population is linear in $N(E_{\rm e},t)$. Thus, it is easy to rescale our results of $N(E_{\rm e},t)$ if we choose other parameters for the acceleration efficiency. We neglect energy loss of thermal ICM due to the acceleration.

For $b(E_{\rm e},t)$, we consider IC scattering of the CMB photons, synchrotron losses, and Coulomb losses. We neglect bremsstrahlung losses for simplicity, which is a good approximation in typical intracluster conditions (Sarazin [13]).

Magnetic field evolution is included by means of the following method. We assume initial magnetic pressure is 0.1 % of ICM thermal pressure. This corresponds to $B = 0.1\mu$G in volume-averaged magnetic field strength. For Lagrangean evolution of B, due to the frozen-in

assumption we apply $B(t)/B(t_0) = (\rho_{\rm ICM}(t)/\rho_{\rm ICM}(t_0))^{2/3}$. Field changes due to the passage of the shock waves is not considered in this paper. The change may depend on field configuration at the shock front and have value of $\sim 1-4$. However, it is difficult to examine it in the present simulation even under high β condition. We will try this problem in the future paper.

Our model implies continuous production of power law distributed relativistic electrons at around the shock fronts. This is valid only when $\Delta t_{\rm acc}$ is sufficiently shorter than the dynamical timescale of the system ($\sim 10^9$ yr), where $\Delta t_{\rm acc}$ denotes acceleration time in which $Q(E_{\rm e}, t)$ becomes power law distribution. It is presented in the framework of the standard shock acceleration theory as $\Delta t_{\rm acc} = 3ru^{-2}(r-1)^{-1}(\kappa_1 + r\kappa_2)$, where u is the flow velocity of the upstream of the shock front, and $\kappa_{1,2}$ are diffusion coefficients of the upstream and downstream, respectively. Assuming $B_1 = B_2$ and Bohm diffusion approximation,

$$\Delta t_{\rm acc} = 1.9 \times 10^2 {\rm yr} \left(\frac{E_{\rm e}}{\rm GeV}\right) \left(\frac{\eta}{10^2}\right) \left(\frac{u}{10^3 {\rm km\ s^{-1}}}\right)^{-2} \left(\frac{B}{\mu {\rm G}}\right)^{-1}. \quad (2)$$

This value is certainly much shorter than the dynamical timescale.

3 RESULTS

Figure 1 shows the time evolution of non-thermal emission for various energy band: from top to bottom, IC emission of the Extreme Ultraviolet Explorer (EUVE) band (65-245 eV), soft X-ray band (4-10 keV), and hard X-ray band (10-100 keV), and synchrotron radio emission (10 MHz - 10 GHz). The times are relative to the most contracting epoch. The calculation of the luminosity for each band is performed in the simplified assumption that electrons radiate at a monochromatic energy given by $E_{\rm X} = 2.5{\rm keV}(E_{\rm e}/{\rm GeV})^2$ and $\nu = 3.7{\rm MHz}(B/\mu{\rm G})(E_{\rm e}/{\rm GeV})^2$ for IC scattering and synchrotron emission, respectively. Since cooling time is roughly proportional to $E_{\rm e}^{-1}$ in these energy range, the higher the radiation energy of IC emission is, the shorter duration of luminosity increase is. In other words, luminosity maximum comes later for lower energy band. Hard X-ray and radio emissions come from the electrons with almost the same energy range. The luminosity maximum in the hard X-ray band, however, comes slightly after the most contracting epoch. On the other hand, radio emission becomes maximum at most contracting epoch since the change of magnetic field due to the compression and expression plays an more crucial role than the increase of relativistic electrons. In any cases, radio halos and hard X-ray are well associated to merger phenomena. They are observable only when thermal ICM have definite signatures of mergers such as complex temperature structures, non-spherical and elongated morphology, or substructures. Soft X-ray emission, which is observable only in clusters (or groups) with relatively low temperature ($\simeq 1$ keV) ICM, is still luminous in ~ 1 Gyr after the merger. Thus, the association of mergers in this band is weaker than in the hard X-ray band. Moreover, EUV emission continues to be luminous after the signatures of the merger have been disappeared in the thermal ICM.

Figure 2 shows the snapshots of synchrotron radio (10MHz-10GHz) surface brightness distribution (solid contours) and X-ray one of thermal ICM (dashed contours) seen from the direction perpendicular to the collision axis. Contours are equally spaced on a logarithmic scale and separated by a factor of 7.4 and 20.1 for radio and X-ray maps, respectively. At $t = -0.25$, the main shocks are located between the two X-ray peaks and relativistic electrons are abundant there. Thus, the radio emission peak is located between the two X-ray peaks although the magnetic field strength there is weaker. At $t = 0.0$, relativistic electrons are concentrated around the central region since the main shocks are nearly standing and located near $X \simeq \pm 0.2$. Furthermore, gas infall compress ICM and the magnetic field. Thus, radio distribution shows rather strong concentration. In these phase (at $t = -0.25$ and 0.0), the radio halo is located at the high temperature region of ICM. On the other hand, at $t = 0.25$, relativistic electron distribution

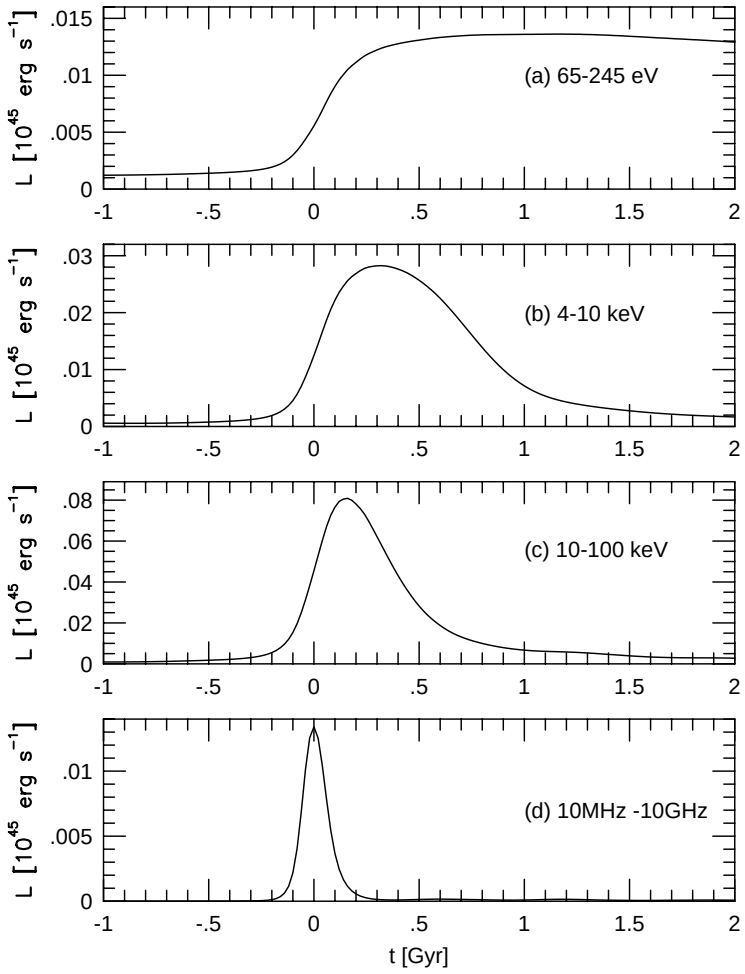

Figure 1: The time evolution of non-thermal emission for various energy band: from top to bottom, inverse Compton scattering of EUVE band (65-245 eV), soft X-ray band (4-10 keV), and hard X-ray band (10-100 keV), and synchrotron radio emission (10 MHz - 10 GHz). The times are relative to the most contracting epoch.

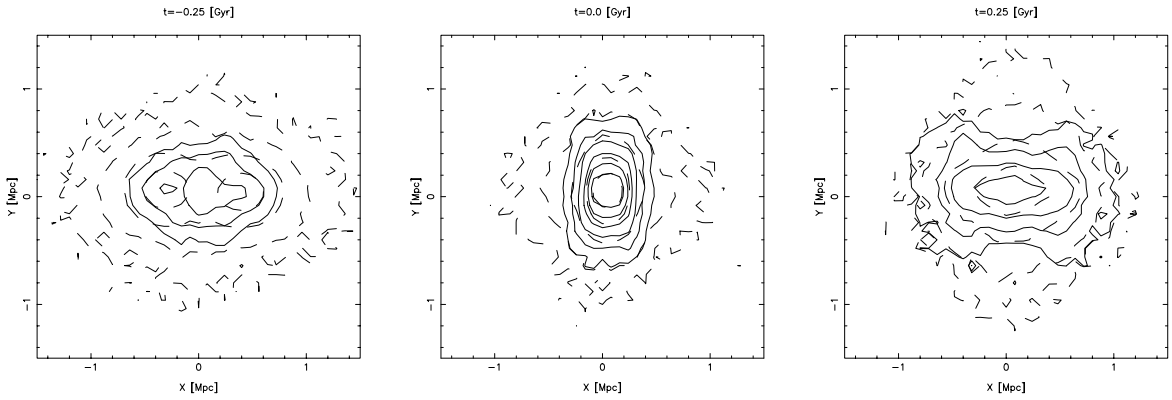

Figure 2: Snapshots of synchrotron radio (10MHz-10GHz) surface brightness distribution (solid contours) and X-ray one of thermal ICM (dashed contours) seen from the direction perpendicular to the collision axis. Contours are equally spaced on a logarithmic scale and separated by a factor of 7.4 and 20.1 for radio and X-ray maps, respectively.

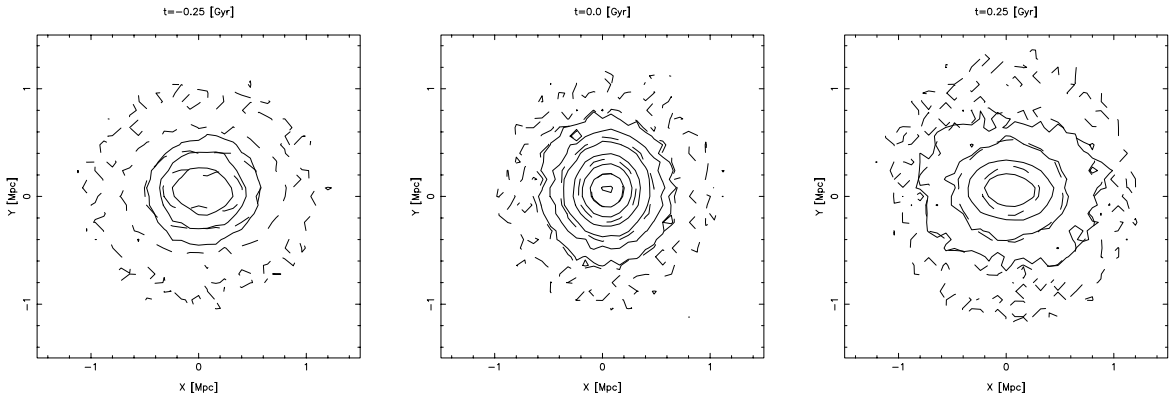

Figure 3: Same as figure 2, but for seen from the direction tilted at an angle of 30° with respect to the collision axis.

becomes rather diffuse since fresh relativistic electrons are producing in the outer regions as the shock waves propagate outwards. At $t = 0.25$ the main shocks are located at $X \simeq \pm 1$. Between the shock fronts rather diffuse radio emission is seen. In this phase, the radio halo is located between two high temperature regions of ICM.

As described above, the morphology of the radio halo is strongly depending on the phase of the merger when viewed from the direction perpendicular to the collision axis. When viewed nearly along the collision axis, however, this is not the case. Figure 3 shows the same as figure 2, but for seen from the direction tilted at an angle of 30° with respect to the collision axis. Radio and X-ray morphology are similar each other in all phases. When the cluster is viewed along the collision axis, the distribution of relativistic electrons roughly follows that of the thermal ICM since the shock fronts face to the observers and spread over the cluster. The distribution of magnetic field strength also roughly follows that of the thermal ICM. Therefor, the radio morphology follows X-ray one.

4 CONCLUSIONS

We have investigated evolution of non-thermal emission from relativistic electrons accelerated at around the shock fronts during merger of clusters of galaxies. Hard X-ray and radio radiations are luminous only while merger signatures are left in thermal ICM. Hard X-ray radiation becomes maximum in the later stage of merger. In our simulation, radio emission is the most luminous

at the most contracting epoch. This is due to the magnetic field amplification by compression. According to the recent magnetohydrodynamical simulations (Roettiger, Stone, & Burns [10]), however, it is possible that the field amplification occurs as the bulk flow is replaced by turbulent motion in the later stages of merger. If this is effective in real clusters, radio emission can increase by a factor of two or three than our results in the later stages of merger. EUV emission is still luminous after the merger signatures have been disappeared in thermal ICM. This is consistent with the EUVE results.

References

1. B. M. Deiss, *et al*, *Astron. Astrophys.* **321**, 55 (1997)
2. Y. Fukazawa, *Astron. Nachr.* **320**, 197 (1999)
3. R. Fusco-Femiano, *et al*, *Astrophys. J.* **513**, L21 (1999)
4. G. Giovannini, *et al*, *Astrophys. J.* **406**, 399 (1993)
5. C. Ishizaka and S. Mineshige, *Publ. Astron. Soc. Jpn.* **48**, L37 (1996)
6. R. Lieu, M. Bonamente and J. P. D. Mittaz, *Astrophys. J.* **517**, L91 (1999)
7. M. Markevitch, C. L. Sarazin and A. Vikhlinin, *Astrophys. J.* **521**, 526 (1999)
8. T. Naito, *et al*, *Astron. Nachr.* **320**, 205 (1999)
9. Y. Rephaeli, *Astrophys. J.* **227**, 364 (1979)
10. K. Roettiger, J. M. Stone and J. O. Burns, *Astrophys. J.* **518**, 594 (1999)
11. K. Roettiger, J. O. Burns and J. M. Stone, *Astrophys. J.* **518**, 603 (1999)
12. H. J. A. Röttgering, *et al*, *Mon. Not. R. Astron. Soc.* **290**, 577 (1997)
13. C. L. Sarazin, *Astrophys. J.* **520**, 529 (1999)
14. S. Schindler & E. Müller, *Astron. Astrophys.* **272**, 137 (1993)
15. M. Takizawa, *Astrophys. J.* **520**, 514 (1999)
16. M. Takizawa and T. Naito, *Astrophys. J.* **535**, 586 (2000)
17. T. Tanimori,*et al*, *Astrophys. J.* **497**, L25 (1998)
18. M. Watanabe, *et al*, *Astrophys. J.* **527**, 80 (1999)